1998

Observations of the diffuse near-IR sky emission with a balloon-borne infrared telescope (TRIP)

N. Mandolesi

M. R. Attolini

S. Cortiglioni

Bruce Partridge
Haverford College, bpartrid@haverford.edu

1998

Observations of the diffuse near-IR sky emission with a balloon-borne infrared telescope (TRIP)

N. Mandolesi

M. R. Attolini

S. Cortiglioni

R. Bruce Partridge
Haverford College

Astron. Astrophys. 331, 463–470 (1998)

ASTRONOMY
AND
ASTROPHYSICS

Observations of the diffuse near-IR sky emission with a balloon-borne infrared telescope (TRIP)

N. Mandolesi[1,⋆], M.R. Attolini[1], S. Cortiglioni[1], G. Morigi[1], L. Valenziano[1], G. Ventura[1], A. Boscaleri[2], A. Franceschini[3], L. Danese[4], and R.B. Partridge[5]

[1] Istituto T.E.S.R.E., CNR, I-40126 Bologna, Italy
[2] I.R.O.E., CNR, Firenze, Italy
[3] Dipartimento di Astronomia, Università di Padova, Italy
[4] Sissa, Trieste, Italy
[5] Haverford College, Haverford, USA

Received 26 June 1997 / Accepted 3 November 1997

Abstract. The diffuse sky emission in 7 spectral bands between 2 and 4.6 microns has been observed with a cooled balloon-borne IR telescope (TRIP). The results, reported here, confirm state-of-the-art atmospheric models for the continuum emission at $\lambda > 3\ \mu$m and for the OH component at $\lambda < 2.3\ \mu$m. On the other hand, excess flux in the 2.3 to 2.5 μm atmospheric window is found at a level of $\lambda I_\lambda \simeq 1.5 - 2\ 10^{-10}$ W cm^{-2} sr^{-1}. Given its modulation with the zenith angle, this signal can be attributed to residual atmospheric emission, possibly due to narrow saturated absorption lines. The sky brightness detected by TRIP in the atmospheric window is 1.5 magnitude fainter at balloon altitudes than the typical sky brightness at South Pole. However, in optimal atmospheric conditions, the sky brightness at South Pole can be only half a magnitude brighter.

Key words: atmospheric effects – diffuse radiation – methods: observational

1. Introduction

Sensitive near-infrared observations from high-altitude sites or from space observatories are suited to test astrophysical processes occurring in the distant universe. The larger are the redshift and the extinction due to intervening or associated dust and gas, the greater is the fraction of the optical-UV photons emitted by primeval objects, reprocessed by dust and gas, now observable at $\lambda > 1\ \mu$m as near-IR background emission.

The near-IR domain is well suited to the exploration of the universe at high redshifts and particularly to search for the light from primeval galaxies. A phase of enhanced star-formation in spheroidal galaxies at high redshifts is called for by various independent arguments (see e.g. Franceschini et al. 1994), including the observed large amounts of metals in the intra-cluster medium (Loewenstein & Mushotzky 1996), of metals and dust in high-z quasars (Franceschini & Gratton 1997), and the tentatively detected sub-mm background (Puget et al. 1996).

In order to detect these faint individual sources, very large photon collectors and extremely sensitive devices are needed. Ambitious projects are aimed at the exploration of these early epochs, in particular the NGST, presently under study, and the Polar Stratospheric Telescope, see Bely et al. 1995. But interesting information on primeval objects can also be given by observing the near-IR cosmological background with small, cooled, low-emissivity IR telescopes through the 2.4 μm atmospheric window in high-altitude terrestrial sites or on board of balloon platforms.

We report here on results of a balloon experiment aimed at the exploration of the near-IR sky emission at 38 Km altitude with a cooled 25 cm telescope, to probe the residual atmospheric signal.

Particular care has been devoted to keep the instrumental noise to a minimum, by cooling the telescope's focal plane to 50 K with a newly developed liquid-helium system and by optimizing the stray-light reduction.

Our results on the atmospheric emissivity in the whole near-IR domain, and in the 2.4 μm window in particular, will significantly impact on projects aimed at implementing large telescopes on stratospheric or balloon-borne platforms for cosmological purposes.

2. Observations

2.1. Experimental set-up

The detection system is based on a cryogenically cooled telescope (a cylinder 1.2 m high, 0.42 m diameter) housing double

Send offprint requests to: N. Mandolesi
⋆ CNR-Tesre, via P. Gobetti 101, I-40126 Bologna, Italy

Cassegrain optics with an F/2 focal ratio and a 25 cm primary mirror.

The focal plane detector was a 32 pixel linear InSb array with fairly good quantum efficiency in the range 1-5 μm (Q.E.=0.8 at 4 μm) and acceptable noise performance when thermalized at about 50 K. The pixel field of view was about 1.4 arcmin, with 90% of light inside the pixel area.

The payload is provided with azimuth and zenith control systems, which independently controlled and stabilized the telescope hour and elevation angle. All payload subsystems, which were continuously monitored and remotely controlled during the flight, operated as expected. In particular, the focal plane detector temperature was stabilized at (52.00 $\pm$ 0.02) K over time scale of a few minutes by the cryogenics control system (Morigi et al. 1996), ensuring homogeneous and reliable data sets.

A complete description of the experimental set-up is given in Ventura et al. (1995) and Morigi et al. (1996).

2.2. The mission

The flight took off at Palestine (Texas) in June 1995 and the payload was floating at an altitude of 38 km for 7 hours during nighttime. The programming strategy was based on multiple sky scans at various azimuth and zenith positions with seven filters. Measurements at different zenith angles in particular are needed to disentangle signals of atmospheric origin. Multiple exposures were performed at any sky position and for any filter so as to reduce statistical errors.

Four successive zenith scans at different azimuth positions and with seven filters have been performed. Fig. 1 schematically shows the TRIP sky coverage during the flight.

Scans 1 and 2 suffered from stray illumination due to the presence of the Moon reflected into the telescope from the balloon surface. Scans 3 and 4, performed in the second part of the flight, were uncontaminated by this effect and gave the most reliable scientific data.

The in-flight calibration activities mainly consisted of:

- calibration of the pointing systems (aspect sensor data), by tracking the Moon in the first part of the flight and by detection of 10 known stellar objects;
- absolute calibration of the detector (including the optics) with several filters, which was based on catalogued IR fluxes of three stars tracked during the flight (βAnd, ϵPeg and β Cap).

2.3. Calibrations and data reduction

In-flight calibrations of the azimuth and zenith control systems allowed us to correct the raw aspect data and to determine the overall precision of the sky position measure. The error box associated to any observed sky direction is $\pm$1 deg in azimuth and $\pm$0.5 deg in zenith.

Absolute in-flight calibrations led to a quantitative evaluation of both the sensitivity of the detector system in operating conditions and the efficiency of the optics at various wavelengths. The in-flight data confirmed both the on-ground calibrations and the data collected during the balloon ascent (the lid closing the telescope before the float altitude was reached acted as a blackbody at a known temperature).

Raw detector data were provided with a series of continuously monitored *house keeping* parameters (focal plane temperature, dark current, DC offsets, readout noise, etc.), so as to allow us to check the working conditions and to correct for instrumental features (e.g. possible drifts during the exposures).

Array detector calibrations were periodically performed to evaluate the in-flight dark current and the intrinsic readout noise. To this aim, each observing schedule included sequences of detector readouts, using different exposure times (between 1 ms and 60 s), with a cold diaphragm blocking the detector aperture.

Raw data for each pixel of the detector and for each individual observed sky position have been averaged. The global uncertainty on resulting brightness value includes instrumental errors (detector dark current, readout noise, detector and electronic gains), absolute calibration errors (optics efficiency) and statistical dispersion of observed data. Errors on Figs. 2,3 and 4 range between 4% and 8%, depending on the observed band. For details on the different contributions to instrumental errors see Ventura et al. (1995).

3. The atmospheric emission

The TRIP observing wavebands have been selected to precisely monitor the atmospheric contribution. Assuming the atmosphere is stratified in parallel layers, its emission is expected to exhibit a dependence on sec θ, where θ is the zenith angle:

$$I(\theta) = I_{\rm isot} + I_{\rm atm} \sec\theta. \quad (1)$$

Here $I_{\rm isot}$ is an unknown isotropic emission term and $I_{\rm atm}$ is the atmospheric emission. Measurement were performed by scanning at different zenith angles and this functional dependence, with two independent parameters, was fitted to the data.

Note that, in any case, data at small zenith angle θ ($\theta < 40^\circ$) in all filters may be affected by a residual contamination of light reflected by the balloon surface. This contamination, which has been clearly detected at $\theta \simeq 28^\circ$, is negligible for angles $\theta \geq 46^\circ$. To avoid bias we excluded the $\theta = 28^\circ$ data from the analysis and we regarded those at θ=39° as upper limits only.

Results from our most sensitive scans 3 and 4 are reported in Table 1.

The TRIP filters can be usefully separated into three wavelength ranges, according to the main contributors to the observed emission: an *OH airglow region* at shorter wavelengths ($\lambda \leq 2.3\,\mu$m); a *thermal IR region* at longer wavelengths ($\lambda > 2.6\,\mu$m) and an atmospheric window centered around $\lambda = 2.4\,\mu$m.

3.1. The thermal IR spectral region

Two bands, centered at 3.54 μm and 4.61 μm respectively, are specifically devoted to monitoring atmospheric emission. At these wavelengths significant contributions to the sky signal

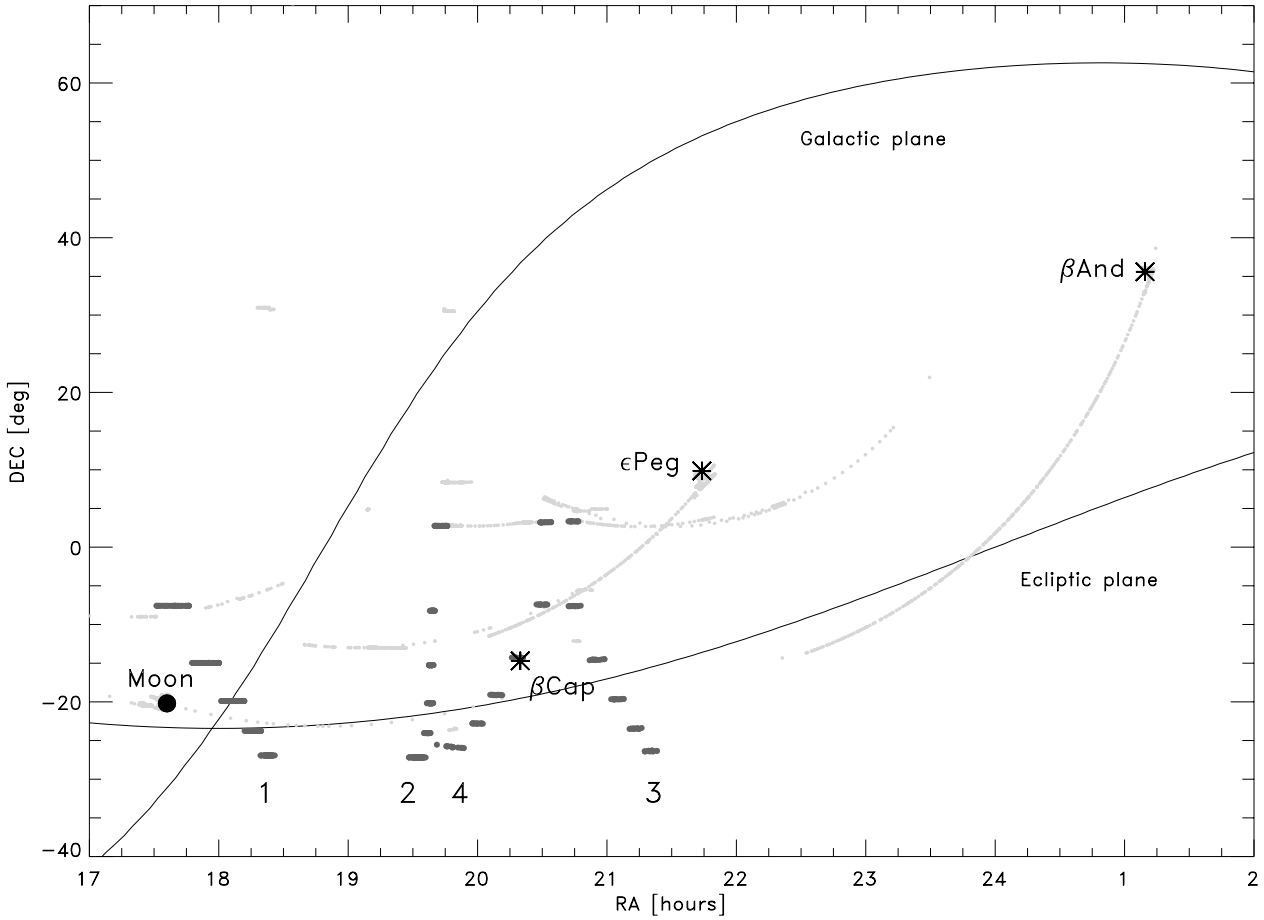

Fig. 1. Sky coverage the TRIP relative to the June 13, 1995 flight.

Table 1. Results from the TRIP 1995 flight

λ (μm)	$\Delta\lambda$(μm)	$I_{\rm atm}$ [W/cm^{2}sr]	$I_{\rm isot}$ [W/cm^{2}sr]
2.025	0.08	$(1.8 \pm 0.06)\ 10^{-9}$	–
2.15	0.10	$(2.9 \pm 0.10)\ 10^{-9}$	–
2.28	0.10	$(1.7 \pm 0.07)\ 10^{-9}$	–
2.39	0.12	$(2.4 \pm 0.31)\ 10^{-10}$ (1)	$< 1.4\ 10^{-10}$
		$(1.6 \pm 0.21)\ 10^{-10}$ (2)	
2.50	0.13	$(2.2 \pm 0.30)\ 10^{-10}$ (1)	$< 1.7\ 10^{-10}$
		$(1.7 \pm 0.21)\ 10^{-10}$ (2)	
3.54	0.12	$(1.78 \pm 1.1)\ 10^{-9}$	$(4.0 \pm 2.0)\ 10^{-9}$
4.61	0.08	$(2.69 \pm .13)\ 10^{-8}$	$(1.07 \pm .03)\ 10^{-7}$

(1) Zenith value of the atmospheric emission measured during scan 4
(2) Zenith value of the atmospheric emission measured during scan 3

come from several atmospheric molecules, such as H_2O, O_2, O_3, CO_2 and others.

We show in Fig. 2 the observed emission at λ=3.54 μm and 4.61 μm as function of the zenith angle. While the data at λ=3.54 μm show some scatter around the secant law, the data at λ=4.61 μm match the expected angular dependence well.

As shown in Table 1, a significant residual isotropic contribution $I_{\rm isot}$ is found when fitting Eq. (1) to the TRIP fluxes in these two wavebands. A fit of this residual is obtained with a black-body emission at a temperature of 193 K with 5% emissivity, which we attribute to thermal emission of the upper part of the telescope body.

The results for the atmospheric emission, reported in Fig. 5 below, turn out to be in agreement with the reference spectrum obtained from the LOWTRAN atmospheric code (Kneizys et al. 1988).

Previous measurements in this wavelength range have been performed by Hofmann et al. (1974) from a balloon at 32 Km altitude at 2.7 and 3.4 μm. While their measurement at 2.7 μm is close to the prediction of the LOWTRAN code (Kneizys et al., 1988), at 3.4 μm it is is significantly higher than both the model prediction and our result at 3.54 μm. The whole discrepancy is not likely accounted for by the lower altitude attained by their balloon flight or by the different band, and is probably affected by thermal emission of the telescope lens. This emission changed by a factor 3 during the flight, and the minimum value was of the same order of the claimed atmospheric emission.

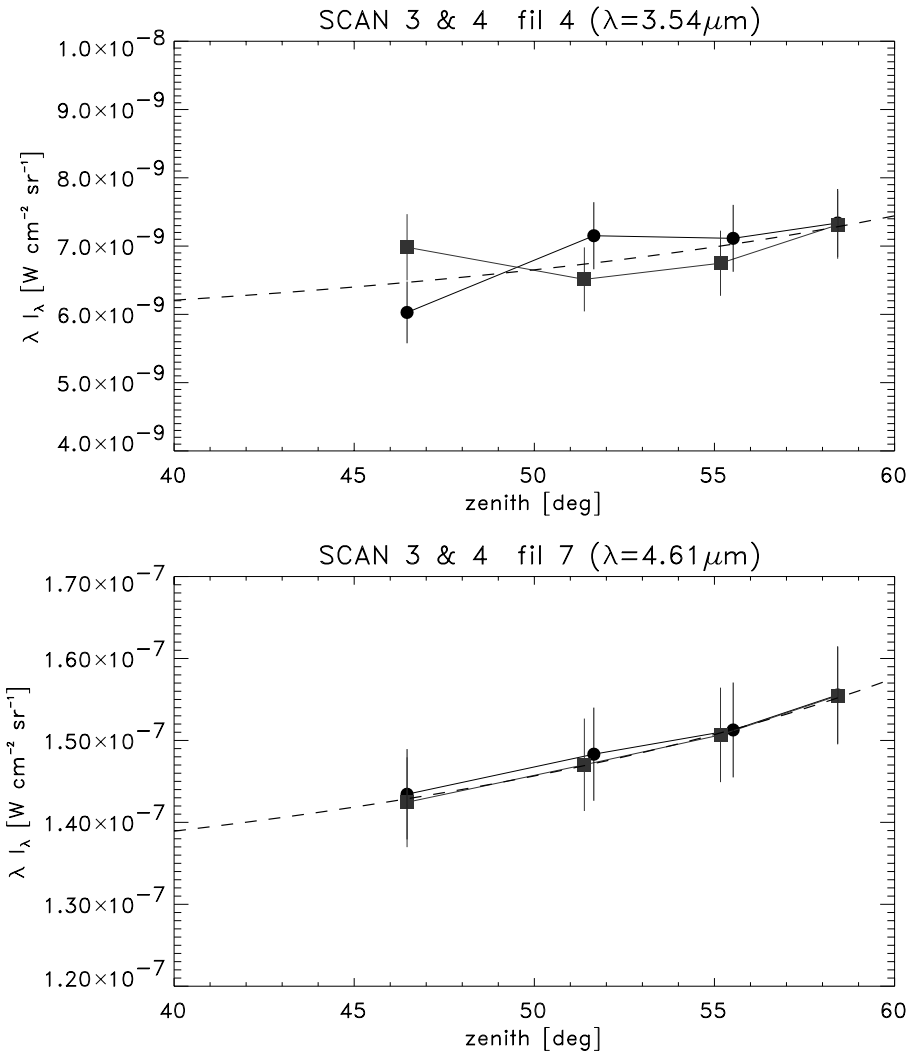

Fig. 2. Zenith scans and secant law modulations (dashed lines): filters 4,7 dominated by continuum atmospheric emission. Two TRIP scans are reported: circles = scan 3; squares = scan 4

3.2. The OH emission spectral region

The TRIP bands centered at 2.025, 2.15 and 2.28 μm are dominated by OH emission, mainly distributed in the highest atmospheric layers, between 80 and 100 km. Our results are shown in Fig. 3, for the two most sensitive scans of the 1995 flight. These data have been analysed as in the previous section, but instead of a simple secant law we applied a Van Rhijn's law (Van Rhijn 1921), which better describes emission by molecules distributed in thin, outer atmospheric layers. We report the results of fitting the scan 3 only, while scan 4 data are plotted to show the scatter, which is likely to attribute to time variability in OH airglow emission.

The OH emission is detected at high significance and the zenith values are reported in Table 1. Any possible isotropic components turn out to be a negligible fraction of the total observed emission at these three wavelengths (the predicted brightness of the Zodiacal and Starlight in the observed sky regions at these wavelengths are well below the detected flux).

A comprehensive compilation of available balloon data for observations before 1994 can be found in Matsumoto et al. (1994). Also of interest are observations of the near-infrared sky from the South Pole by Ashley et al. (1996) and Nguyen et al. (1996).

A straightforward comparison is possible, in particular, between our result at λ = 2.15 μm and the one by Hofmann & Lemke (1977) at 2.1 μm (the observations have been performed at similar altitudes). As appearing in Fig. 5, the agreement between TRIP observations (black filled circles) and Hofmann results (open red triangles) is very good.

Spectroscopic observations have been performed from a balloon floating at 27 Km altitude by Gush & Buijs (1964). Translating their spectroscopic results, Matsumoto et al. (1994) reported a value of 13×10^{-9} W cm^{-2}sr^{-1} at 2.00 μm, significantly higher than our findings. However the transformation of narrow-band into broad-band data is rather uncertain in the case of sparsely sampled spectroscopy.

Finally, it is worth noticing that Ashley et al. (1996) measured the sky brightness from the Amundsen–Scott South Pole Station in the range 1.4–2.5 and 2.9–4.2 μm with circular variable filters at a resolution of 1%. At 2.0 μm their result is a factor about 3 below the value claimed by Gush & Buijs (1964) and a

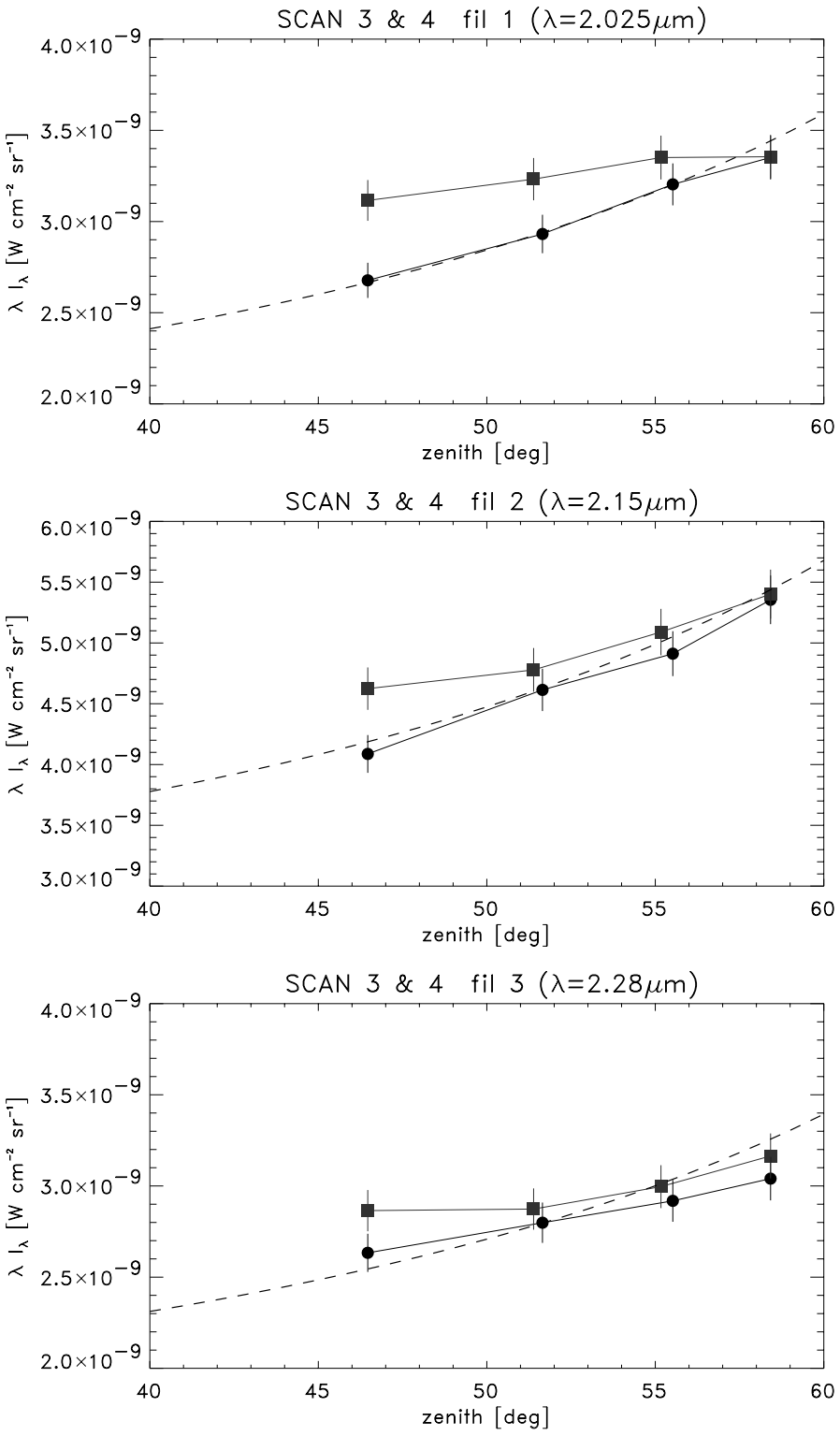

Fig. 3. Zenith scans and Van Rhijn law modulations (dashed lines): filters 1,2,3 dominated by atmospheric OH emission. Symbols as in Fig. 2

factor of 2.5 higher than our result after proper convolution. The sky brightness over the South Pole is $\simeq 4 \times 10^{-9}$ W cm^{-2} sr^{-1} at 2.15 μm and $\simeq 10^{-9}$ W cm^{-2} sr^{-1} at 2.28 μm, i.e. 40% more and 70% less than our results respectively.

The independence of the sky brightness on the altitude (at least up to 40 Km) confirms that the atmospheric emission is dominated by the OH airglow in this band. However, full understanding of the whole dataset is not straightforward. A dependence of the OH airglow on the observation site is a possibility. In addition, time variability is also likely to be present. Indeed, we do find significant brightness fluctuations between scans 3 and 4 in our flight.

In any case, all observations agree on the fact that beyond 2.3 μm the OH airglow emission is significantly decreasing.

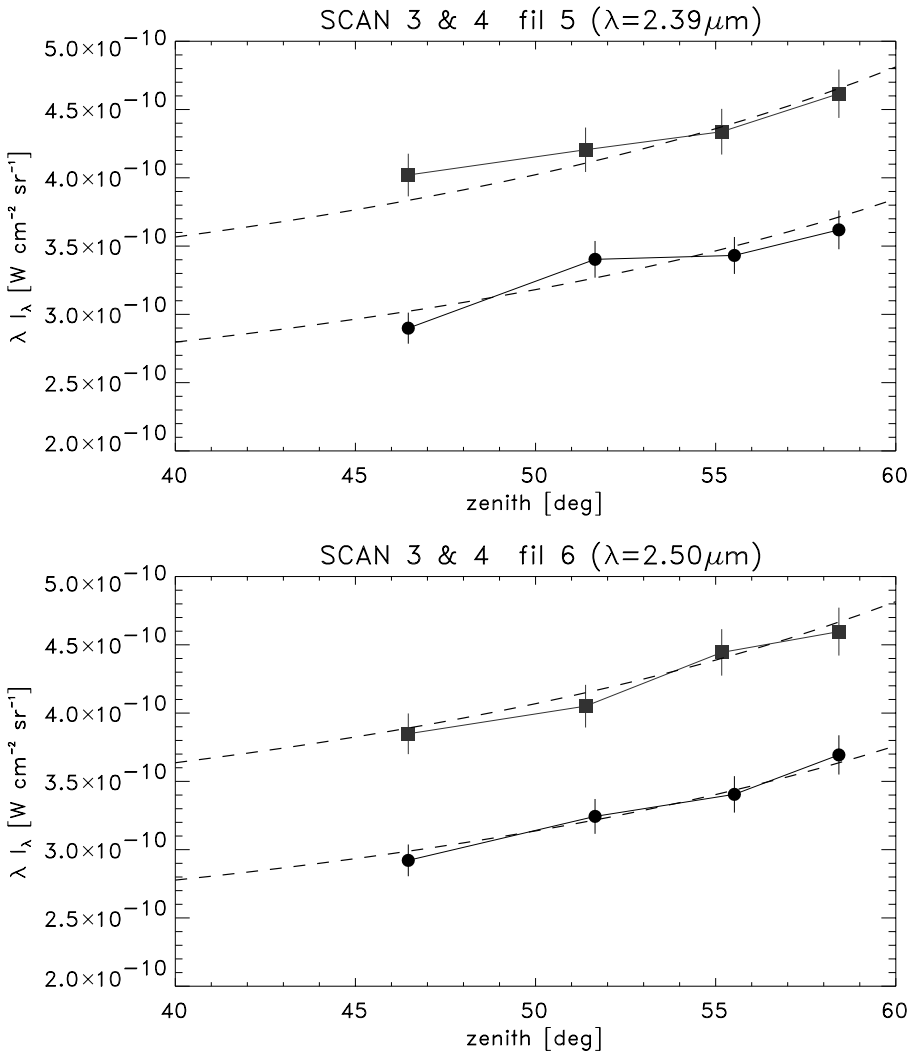

Fig. 4. As Fig. 3, but for filters 5,6 in the $\lambda = 2.3 - 2.6$ atmospheric window

3.3. Emission in the atmospheric window at 2.4 μm

In these bands we expect a minimum residual contribution from the atmosphere and the OH airglow. In Fig. 4 we present the data obtained at 2.39 and 2.50 μm during scans 3 and 4. It is apparent that during scan 4 the measured emission was $\simeq$ 25% higher than in scan 3. The statistical analysis shows that the variation can be ascribed to the component which follows a secant-law dependence on the zenith angle, i.e. to the Earth's atmospheric emission. The significance of the result is very high, since $\chi^2 \sim 1$ under the assumption of different atmospheric emission in the two scans (3 degrees of freedom), whereas $\chi^2 \sim 40$ under the hypothesis of a single atmospheric emission (2 dof). Also the correlations between the emissions observed at λ =2.39 and 2.50 μm (see Fig. 4) support a real variation of the atmospheric signal during the two scans.

Again the variation may possibly be attributed to both temporal and spatial fluctuations of the atmospheric emission. The two estimates of the atmospheric emission for scan 3 and 4 are separately reported in Table 1.

Sky brightness measured by TRIP confirm that there is an appreciable atmospheric emission even in the 2.4 μm window. Our flux measurements turn out to be quite close to the upper limit set in this band by Hofmann & Lemke (1977) on the basis of data collected at 32 Km altitude, but significantly lower than the sky brightness measured from a balloon floating at 27 Km by Matsumoto et al. (1994).

On the other hand, measurements by the two mentioned independent South Pole experiments (Ashley et al. 1996; Nguyen et al. 1996) showed that in the 2.4 μm window the sky brightness varies from 2.6 to 13×10^{-10} W cm^{-2} sr^{-1}. At present the origin of this variability is not understood. However the minimum value found is quite close to the emission detected by TRIP at 40 Km.

It is worth noticing that models of the Earth's atmosphere including OH airglow predict significantly lower brightness (Harper 1989)

Our data at 2.5 μm show a variability which closely follows that observed in the 2.4 μm band, suggesting a related origin for such atmospheric signal. Unfortunately there are no available measurements to be compared with our results in this band. The

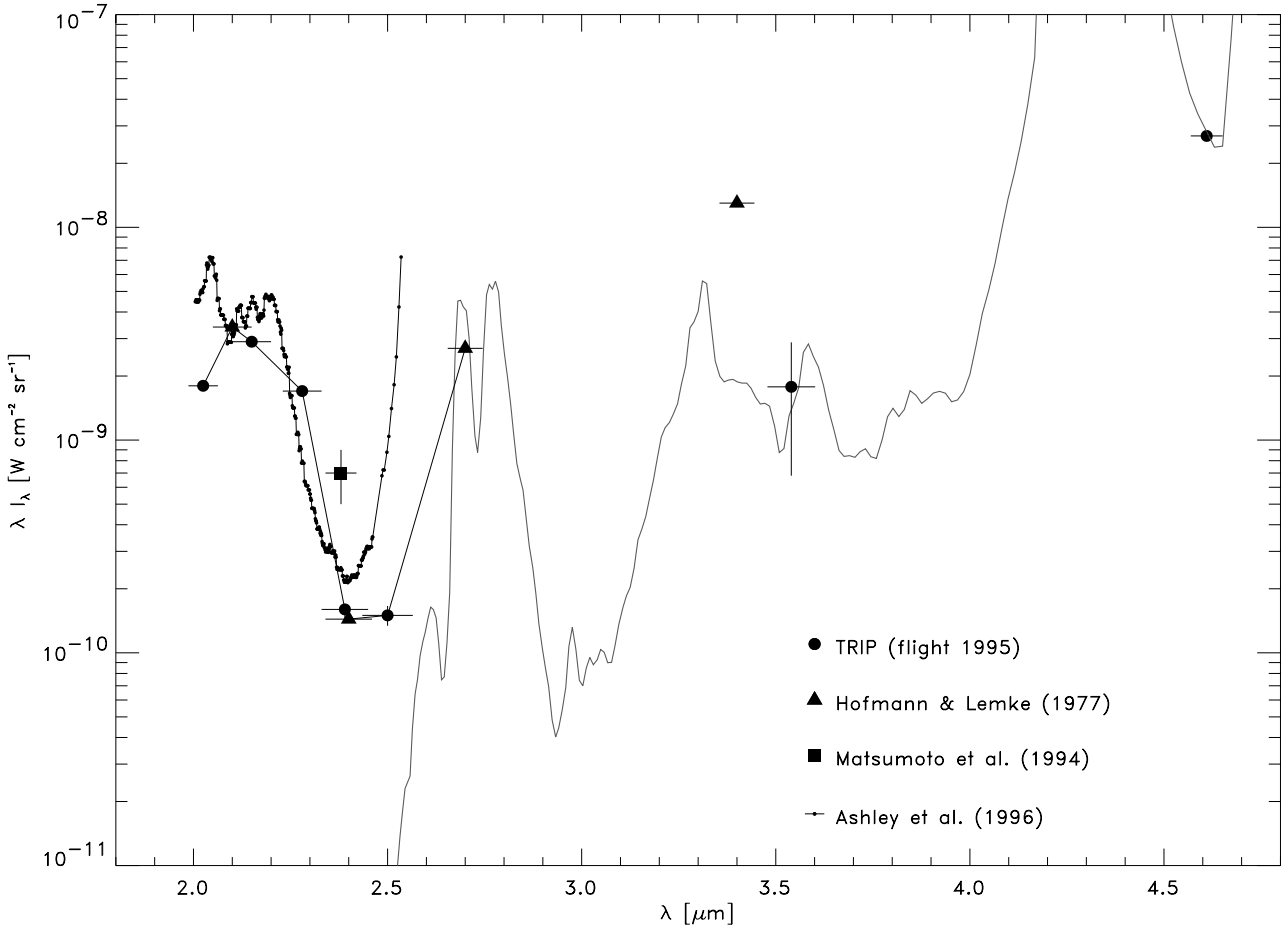

Fig. 5. Atmospheric emission at the zenith, compared with a model atmosphere at the TRIP floating altitude (38 Km). Triangles are measurement by Hofmann & Lemke (1977), the filled square is by Matsumoto et al. (1994), solid line is by Ashley et al. (1996). Note the good agreement between TRIP results at 2.1 μm and Hofmann & Lemke one at 2.15 μm. Data from Ashley et al. (1996) represent the best conditions at the South Pole during winter time and should be considered as lower limits to the sky brightness measured from a ground site. Plotted brightness errors for each band refer to formal errors found from the fitting procedures of the observed brightness data.

measurements of Ashley et al. (1996) clearly exhibit a steep rise at $\lambda = 2.5$ μm and longwards, consistent with an atmosphere at about 230 K and emissivity 0.1, and hence are not comparable to our results.

In conclusion, the 2.4 μm window is not completely free of emission from the Earth's atmosphere at 38 Km altitude. This emission has been clearly detected by TRIP, and varies possibly because of spatial and temporal fluctuations. The zenith sky brightness detected by TRIP is rather close to the minimum detected by two independent experiments performed at Amundsen–Scott South Pole Station during winter season.

In the sky regions observed by TRIP, we have analysed DIRBE data and we have found a sky brightness $\lambda I_\lambda \simeq 5.5 \times 10^{-11}$ W cm^{-2} sr^{-1} mainly contributed by Zodiacal and Star-light from our Galaxy, but possibly including also an extragalactic contribution. Our data in the 2.4 μm atmospheric window have been analysed both allowing for an isotropic contribution, as well as fixing it at the DIRBE measured level. When the isotropic component is treated as a free parameter, a best-fit is obtained with values very close to the DIRBE results. Because of limited sky coverage of TRIP and of the overwhelming atmospheric contribution, only upper limits can be set on the residual isotropic background:

$$\lambda I_\lambda \leq 1.4 \times 10^{-10} \text{ W cm}^{-2} \text{ sr}^{-1} \quad (2)$$

4. Discussion and conclusions

The atmospheric emission and OH airglow have been accurately measured at balloon altitudes by TRIP. The observed atmospheric emission in the thermal region turns out to be in good agreement with the predictions derived by using the LOWTRAN code (Kneizys et al. 1988).

In the wavelength interval dominated by OH emission the published results are rather scattered, due to time and spatial fluctuations. Our results agree with the available data within a factor of 2.

Time fluctuations in the sky brightness by less than a factor of 2 have been found during a single night, and similar fluc-

tuations also appear in data taken on a timescale of a year in observations performed by balloon experiments (Hofmann & Lemke 1977). During our scan 3 and 4 the OH emission was stable, as shown in Fig. 3.

A significant emission from the Earth's atmosphere is found by TRIP in the K-band window at 2.39 and 2.50 μm (see Sect. 3.3). The origin of this flux may be attributed to residual airglow or thermal emission from narrow saturated absorption lines (Nguyen et al. 1996). The observed sky brightness is much larger than that predicted by theoretical models of the OH emission. An interesting feature of this residual is that it varied significantly between scan 3 and scan 4, but there is no counterpart variation in the OH emission at $\lambda < 2.3$ μm. If the observed signal in the K-band window were due to OH lines, then we would expect correlated variations at wavelengths where the emission is dominated by OH. Furthermore, Ashley et al. (1996) and Nguyen et al. (1996) found a typical sky brightness at 3 Km height larger by a factor of 4 than was measured by TRIP at 38 Km. This suggests that the emission is not confined to high atmospheric layers, as it is the case for OH-generated lines. All this supports the conclusion that OH is not the main contributor to the observed emission and that thermal emission from narrow saturated absorption lines is the most probable mechanism.

Concerning the extraterrestrial background, our data on the residual atmospheric signal in the 2.3 to 2.5 μm window is still a factor ≥ 3 larger than the expected Zodiacal and Starlight, which obviously hampers any efforts to measure the IR background from balloon platforms.

Finally, the comparison between data from the South Pole Amundsen-Scott Station and ours confirms that South Pole is a very good site for telescopes operating in the 2.3-2.5 μm band. While the typical sky of the South Pole is 1.5 magnitude brighter, in optimal winter conditions it is only 0.5 magnitude brighter than the sky seen by TRIP at 40 Km.

References

Ashley M.C.B., Burton M.G., Storey J.W.V., et al., 1996, PASP 108, 721

Bely P.Y., Ford H.C., Burg R., et al., 1995, POST: POlar Stratospheric Telescope, 1996. In: Thronson H.A. Jr., Sauvage M., Gallais P., Vigroux L. (eds.), "Infrared and Submillimeter Space Missions in the coming decade", Space Science Reviews 74, 101 (Kluwer Academic Publisher)

Franceschini A., Gratton R., 1997, MNRAS 286, 235

Franceschini A., Mazzei P., De Zotti G., Danese, L., 1994, ApJ 427, 140

Gush H.P., Buijs H.L., 1964, Can. J. Phys. 51, 287

Harper D.A., 1989. In: M. Pomerantz (ed.) Astrophysics in Antarctica, AIP Conf. Proc. 198, AIP, New York, p.123

Hofmann W., Lemke D., 1977, A&A 68, 389

Hofmann W., Frey A., Lemke D., 1974, Nat 250, 636

Kneizys F.X., Shettle E.P., Gallery W.O., et al., 1988, User's Guide to LOWTRAN 7, AFGL-TR-88-0177, (NTIS AD A206773)

Loewenstein M., Mushotzky R.F., 1996, ApJ 471, L83

Matsumoto T., Matsuura S., Noda M., 1994, AASP 106, 1217

Morigi G., Ventura G., Mandolesi N., et al., 1996, Rev. Sci. Instr. 67, 10

Nguyen H.T., Rauscher B.J., Severson S.A., et al., 1996, PASP 108, 718

Puget J.-L., Abergel A., Bernard J.-P., et al., 1996, A&A 308, L5

Van Rhijn F.J., 1921, Publ. Astr. Lab. Groningen 31, 1

Ventura G., Malaspina M., Boscaleri A., et al., 1995, Exp. Astr. 6, 59-82

This article was processed by the author using Springer-Verlag LaTeX A&A style file *L-AA* version 3.